Editors' Suggestion

Kinetic Kagome Magnetism: From Self-Trapping RVB Polarons to Semiclassical Correlations

Yufei Pei,[1,2] Shuai A. Chen,[2] Claudio Castelnovo,[1] and Roderich Moessner[2]
[1]TCM Group, Cavendish Laboratory, JJ Thomson Avenue, Cambridge CB3 0US, United Kingdom
[2]Max Planck Institute for the Physics of Complex Systems, 01187 Dresden, Germany

(Received 10 June 2026; accepted 17 July 2026; published 31 August 2026)

To gain deeper insight into the role of hole kinetics in determining magnetism in highly frustrated doped Mott insulators, we consider the single-hole counter-Nagaoka problem on the kagome lattice, using magnetization as a tuning parameter. Near full polarization, a doped hole delocalizes upon binding reversed spins in a pattern of singlet bonds which we term resonating-valence-bond (RVB) polaron. These RVB polarons can have extremely small effective bandwidths, and hence exhibit self-trapping. By tuning the spin polarization, we track the evolution of these states toward the unpolarized sector, where we observe the emergence of $\sqrt{3}\times\sqrt{3}$ antiferromagnetic correlation reminiscent of the classical Potts and Heisenberg models on the kagome lattice. These results provide a framework to understand how RVB physics at short scales evolves into conventional magnetic correlations at long scales.

DOI: 10.1103/zbxv-vtq8

The interplay between itinerant particles and magnetism is a constitutive problem of strongly correlated electron physics. Pioneering work by Nagaoka [1–3] showed that (ferro)magnetic correlations can originate from the kinetic energy of a sufficiently low density of dopants in infinite-U Hubbard systems, where virtual exchange processes are absent. When said kinetic energy is frustrated, it was later shown that antiferromagnetic correlations can also appear [4–7].

Seminal work by Haerter and Shastry [8] set the stage for the study of kinetic antiferromagnetism in many-body systems (see also Ref. [9] for an earlier study). Research efforts to date focused primarily on the two-dimensional triangular lattice, where kinetic frustration leads to 120° antiferromagnetic order [10]. This behavior is in notable contrast with studies on chains [11], Husimi cactus graphs [12], and nonplanar lattices [6,13], where instead the magnetic correlations can be understood in terms of valence bond singlets. Interest and research activities in these systems has seen a substantive resurgence of late, also thanks to advances in computational approaches—in particular density-matrix renormalization group [14–17]—and experimental progress in moiré materials and cold-atomic systems [18–22].

In this Letter we study the prototypical example of such Hamiltonians—a kinetically frustrated singly doped, infinite-U Hubbard model—on the kagome lattice, the archetypical highly frustrated lattice in two dimensions. By progressing through different magnetization sectors, we are able to show how valence bond singlet physics underpins the behavior of the system close to magnetic saturation, leading to the formation of what we dub RVB polarons. As the number of reversed spins increases, resonant processes between overlapping valence bond patterns gradually give rise to magnetic correlations that are consistent with semiclassical $\sqrt{3}\times\sqrt{3}$ order in the unpolarized sector. Our model provides an important conceptual bridge between singlet physics and conventional antiferromagnetism borne out of kinetic frustration.

Interestingly, we find that the polarons formed by holes and reversed spins interplay in a nontrivial way with the localization properties typical of the kagome lattice [23,24]. Indeed, kinetic frustration arises when the kagome flat band happens to be lowest in energy for a hole-doped fully polarized electron system close to half-filling. As such, holes in a fully polarized system occupy compact localized states [24] at low energy. Upon adding few reversed spins, polarons form and delocalize, albeit with a band mass 100 times larger than that of an unfrustrated tight-binding particle on the same lattice. Once the number of reversed spins is large enough for the valence bond pattern to resonate around closed loops, the polarons appear to relocalize, in that the best of our numerics shows a further and sudden increase in band mass of at least a factor of 10^6. Eventually, in the unpolarized limit, the large density of reversed spins succeeds to relieve the kinetic frustration and delocalized, dispersive holes are recovered.

Our Letter uncovers an intricate interplay between single-particle flat bands and cooperative "polaronic" self-trapping physics, as well as between resonating-valence-bond physics and semiclassical magnetic correlations. In this sense, the counter-Nagaoka effect on the kagome lattice presents a variable and dense fabric woven out of various strands of correlated and topological electron physics, whose joint origins lie in the study of high-temperature superconductivity and frustrated magnetism.

Model—We consider the infinite-U Hubbard model on the kagome lattice,

$$\mathcal{H} = -t \sum_{\langle ij \rangle, \sigma} c^{\dagger}_{i\sigma} c_{j\sigma}, \tag{1}$$

where $\langle ij \rangle$ enumerate nearest neighbor sites, and $c^{\dagger}_{i\sigma}$ ($c_{i\sigma}$) are creation (annihilation) operators for electrons with spin $\sigma \in \{\downarrow, \uparrow\}$ at site i, subject to projecting out the states with double occupancy. Kinetic frustration arises when $t > 0$ (set hereafter to $t = 1$ as our unit of energy). This can be seen straightforwardly by solving the two-electron problem on a single triangle, as illustrated in Fig. 1(a). Ferromagnetic spins have lowest energy $E_0 = -t$ due to destructive interference of the hole motion around the triangle; whereas antiferromagnetic spins can form a singlet and effectively thread a π flux through the triangle, relieving the frustration and allowing the hole to delocalize and lower the energy to $E_0 = -2t$ (bottom of an unfrustrated 1D tight-binding band).

In the following we study this system using exact diagonalization (ED: Lanczos [25], XDiag [26]) and density matrix renormalization group (DMRG: TeNPy [27]), in the YC-ones geometry shown in Fig. 1(b) (see also End Matter).

RVB polarons and delocalization—The fully polarized case reduces to a well-known spinless fermionic tight-binding model, where the bottom band is exactly flat (energy -2) and the states [28] are compact localized around individual hexagons [24], see Fig. 1(b).

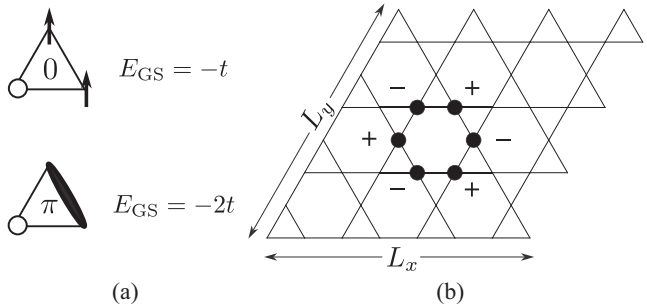

FIG. 1. (a) Kinetic magnetism in the presence of frustration favors the formation of valence bond singlets. (b) Kagome lattice geometry used in our simulations, for system size $N = 3L_xL_y$. We also show an example of a compact localized state around a single plaquette [24].

We begin by studying the behavior of a single hole as we progressively depart from full polarization: 1HnS, where $n = 1, 2, 3, \ldots$ is the number of reversed spins. We observe that the reversed spins cluster around the hole, forming a polaron (akin to the behavior on the triangular lattice [30]). The short distance physics of the kagome lattice is close to tree-like, and we find that the valence bond language of the same Hamiltonian on the Husimi cactus [12] proves highly useful to model and understand the polarons in this Letter, as we demonstrate below. We therefore dub them RVB polarons to contrast them with the different, magnonlike description of polarons on the triangular lattice. The farther one departs from the polarized limit (i.e., the larger n), the less effective the valence bond language is, and the more the magnetic correlations become consistent with semiclassical $\sqrt{3} \times \sqrt{3}$ order.

Remarkably, for $n = 1$, 2, 3, 4 we find that the RVB polarons are delocalized—contrary to the case of $n = 0$—with an enhanced band mass (compared to the 1H1S polaron on the triangular lattice [30]). ED shows a dispersive bottom band that is well fit by an effective unfrustrated tight-binding model with hopping $t_{\text{eff}} \simeq -4.2 \times 10^{-3}$, up to an overall energy offset [see Fig. 2(a) and Supplemental Material [31]]. Note that only two out of the three bands of the 1H1S system

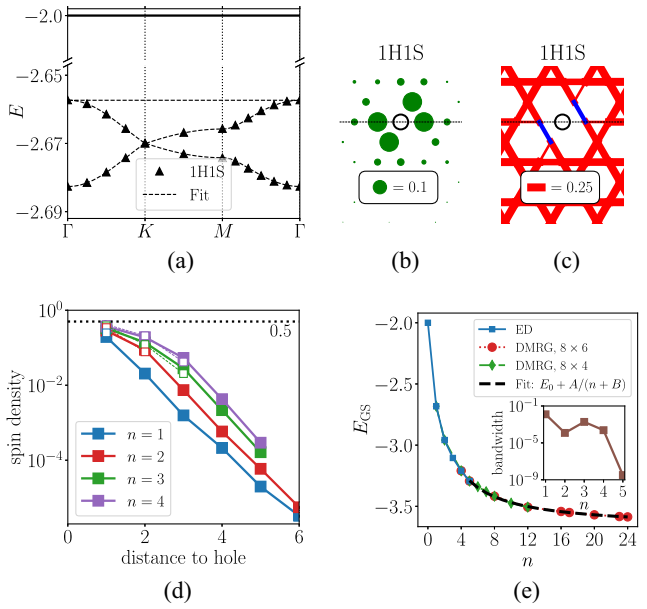

FIG. 2. Band structure for the 1H1S system of size 12 × 12 (a), obtained using ED; the dashed line shows a single-particle tight-binding fit with $t_{\text{eff}} \simeq -4.2 \times 10^{-3}$ and offset $\simeq 2.67$. Spin density (b) and spin correlations (c) (red ferro and blue antiferro, with width proportional to their strength), for fixed hole position. Spin density profile (d) along the horizontal line in panel (b), for 1HnS systems with $n = 1, \ldots, 4$, comparing ED (solid squares) with Husimi cactus cluster results (open squares). The dependence of the GS energy of the 1HnS systems on n is shown in panel (e), with the inset plotting our best estimate for the width of the lowest band from ED (see Supplemental Material [31]).

are captured by the effective model; the third one is exactly flat at $E = -2$, split by a finite gap from the other two.

We look into the magnetic structure of the RVB polarons by computing the spin density and correlations after projecting the hole on a given site of the lattice [see Figs. 2(b)–2(d) and the Supplemental Material [31]]. We are able to interpret these patterns in light of the valence bond behavior on the Husimi cactus [12]: we consider all possible Husimi clusters that are compatible with the lattice and with the number of reversed spins (see Fig. 3 for some examples, and the End Matter for technical details); we then compute the ground state of Hamiltonian (1) on each of these clusters [34], and we use them to create states for the full lattice by taking the tensor product with polarized spins on all other sites. For $n = 1$, 2, 3 the clusters are unique up to lattice symmetries (see Fig. 3), and we find that the resulting states have excellent projection onto the exact ground state (GS) of the full system (88,93,90%, respectively). For $n = 4$ there are three nonequivalent clusters (see Fig. 3), and we find that the star-shaped one has lowest cluster energy and largest projection onto the exact GS (94%). These results show how the structure of the polarons on the kagome lattice is well-described by the local Husimi cactus valence bond physics—hence the name RVB polarons. This is further confirmed by comparing the spin density [empty squares in Fig. 2(d)] and correlators (not shown) obtained from the Husimi cluster states described above and from the exact GS.

These Husimi cluster states have finite hole support by construction. From Fig. 2(d) we see that the actual GS from ED exhibits exponentially decaying tails. The decay length appears to be asymptotically independent of the choice of cluster; it is indeed a property of the compact localized states that govern the physics away from the polaron (where the system is effectively fully polarized). The dispersive nature of the 1HnS lowest-energy bands (for $n = 1, 2, 3, 4$) tells us that the hole is able to move across the lattice whilst carrying such structured polaron along with it. The large band mass suggests that such cooperative motion involves high-order processes and correspondingly small amplitudes.

Strong self-trapping—The behavior of the system changes dramatically for $n \geq 5$. The polaron bandwidth suddenly drops by at least six orders of magnitude ($< 10^{-8}$ in a 4×4 system of 48 sites, with 16 near-degenerate GSs); to the best of our numerics it is indistinguishable from a flat band of localized states. The reversed-spin density appears to be supported by a 12-site cluster symmetrically arranged around a hexagonal plaquette [Fig. 4(a)], while the hole density appears to extend farther [Fig. 4(b)]. Both exhibit a pronounced exponential decay beyond the 12 sites [Fig. 4(c)], as confirmed by DMRG and ED [35]. We find a ratio of approximately 4 between the spin and hole density correlation lengths, which can be qualitatively understood from the fact that reversed spin motion is mediated by hole motion, and it takes an excursion with at least four hole hops starting from the 12-site cluster to

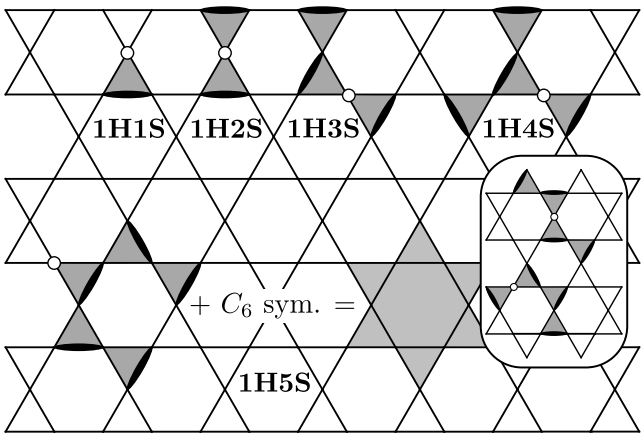

FIG. 3. Examples of Husimi cactus clusters used in the main text to understand the nature of the polarons. All symmetry-inequivalent clusters are shown for 1HnS, with $1 \leq n \leq 4$. For $n = 4$, there are three possible configurations: a star-shaped one shown in the main figure, and two linear ones shown in the inset. For $n = 5$, only the most relevant shape is shown; with its five symmetry-equivalent partners, this shape covers a 12-site (shaded) region of the lattice. For each cluster, only one of the possible hole positions, and its corresponding valence bond arrangement, are shown.

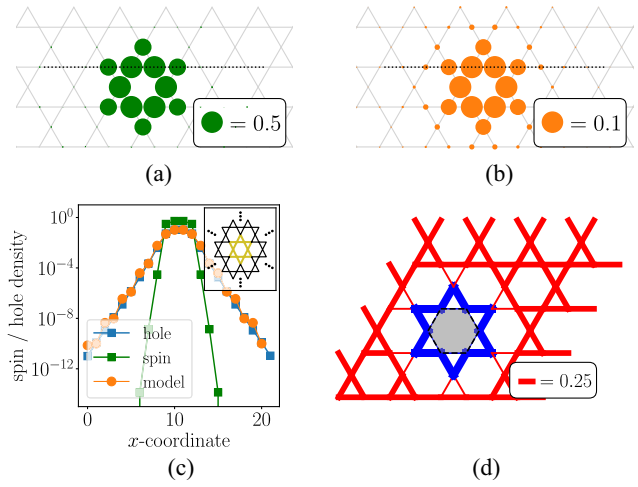

FIG. 4. Reversed spin (a) and hole (b) densities for one of the seemingly localized 1H5S GSs. Profile cuts are shown in panel (c). The hole density is well described by a simple model of a spinless fermion (see inset and main text) with unfrustrated hopping on a 12-site cluster ($t = -1$, yellow edges), embedded on a periodic kagome lattice with frustrated hopping ($t = 1$, black edges). The spin correlators (red for ferro, blue for antiferro) are shown in panel (d), with the thickness of the lines denoting their strength. Density results were obtained using DMRG and spin correlators using ED (see End Matter). A vanishing pinning potential was used to single out a given location for the RVB polaron in the GS.

move a reversed spin out of it. The spin correlators are shown in Fig. 4(d).

To gain insight into the sudden change of behavior of the 1H5S case, we consider again the effective modeling in terms of Husimi clusters employed earlier for $n < 5$. Similarly to $n = 4$, multiple cluster shapes are possible, and their energy is lowest the more ramified their structure. However, for $n = 5$ the most ramified structure does not provide the largest overlap with the exact GS. This is achieved instead by a maximally curved linear arrangement of triangles, illustrated in Fig. 3. This apparent contradiction is explained by the fact that there are six symmetry-related such clusters around any hexagonal plaquette of the lattice, and the corresponding six Husimi cactus states are not orthogonal. By restricting the Hilbert space of the system to the subspace spanned by these six states, and then obtaining the GS of the Hamiltonian within it (see End Matter), we find indeed that the GS energy is lower than that of all other Husimi clusters, and the GS wave function takes the form of a symmetric superposition of all six states, spreading across all 12 sites around the hexagonal plaquette (see Supplemental Material [31]). Its overlap with the exact GS is once again excellent (90%).

By resonating around a hexagonal plaquette, it seems that the 1H5S RVB polaron acquires a possibly infinite mass, undergoing localization reminiscent to the compact-localized hexagonal states of the spinless single-particle problem [24]. Indeed, our results suggest that the reversed spins form a background that allows the hole to delocalize across the 12 sites, whereas its density is heavily suppressed outside of the region. We can then assemble an *ad hoc* tight binding model for a spinless fermion on the kagome lattice, with frustrated hopping ($t = 1$) everywhere except for bonds between the 12 sites, where we set unfrustrated hopping ($t = -1$), see inset of Fig. 4(c). The ground state wave function of this simple toy model has particle density in excellent agreement with the hole density of the original problem, as illustrated by a comparison of density profile cuts in Fig. 4(c).

Unpolarized state and $\sqrt{3} \times \sqrt{3}$ correlations—The study of 1HnS systems with $n > 5$ is beyond the reach of our ED. DMRG results suggest that their behavior is similar to the case $n = 5$ discussed above (see Supplemental Material [31]). Once again we find evidence of a compact support region for the reversed spins, with the hole density also exponentially localized to it—albeit less tightly than the reversed spins [36].

The GS energy is plotted in Fig. 2(e), and shows scaling $\simeq E_0 + A/(n + B)$ at large n (where $E_0 = -3.68 \pm 0.01$, $A = 2.26 \pm 0.13$ and $B = 0.84 \pm 0.23$, from a fit performed over $5 \leq n \leq 24$). This is consistent with the reversed spins forming an effective quantum well confining the hole to a region of linear size $\propto \sqrt{n}$ (n reversed spins live in a region formed by n triangles on the kagome lattice).

As the size of the reversed spin region grows, it encompasses more hexagonal loops of the lattice and the effective modeling in terms of Husimi clusters becomes less and less useful. We see that this "frustration on frustration" leads to the appearance of magnetic correlations consistent with semiclassical $\sqrt{3} \times \sqrt{3}$ order as we approach the unpolarized limit. To show this, we evaluate the structure factor

$$S(\mathbf{k}) = \frac{1}{N^2} \sum_{i,j} \langle \mathbf{S}_i \cdot \mathbf{S}_j \rangle e^{i\mathbf{k}\cdot(\mathbf{r}_i - \mathbf{r}_j)} \tag{2}$$

for the GS obtained either by ED (on a 3×3 system) or by DMRG (on cylinders with $L_y = 3$ and L_x integer multiple of 3). In all cases, we find peaks at the K points, suggestive of $\sqrt{3} \times \sqrt{3}$ order [see Supplemental Material [31] for intensity plots of $S(\mathbf{k})$ in the entire Brillouin zone (BZ)] [37]. We plot the intensities of the peaks multiplied by system size, $NS(\mathbf{k} = K)$ in Fig. 5, showing that $S(\mathbf{k} = K)$ decreases more slowly than $1/N$. For comparison, we present results from classical simulations of the three-state Potts model on systems of equivalent size. This model is useful [38,39] in that it sits at the Kosterlitz-Thouless (KT) transition separating a $\sqrt{3} \times \sqrt{3}$ ordered and an algebraically correlated phase, and it can thus provide a natural benchmark for an analysis of semiclassical correlations. It reflects the low-temperature correlations of a classical XY kagome magnet exactly, and—appropriately perturbed—those of the classical Heisenberg magnet approximately. Its straightforward numerical tractability allows the analysis of systems of the finite sizes to which our other numerical methods are restricted. The Potts model exhibits similar

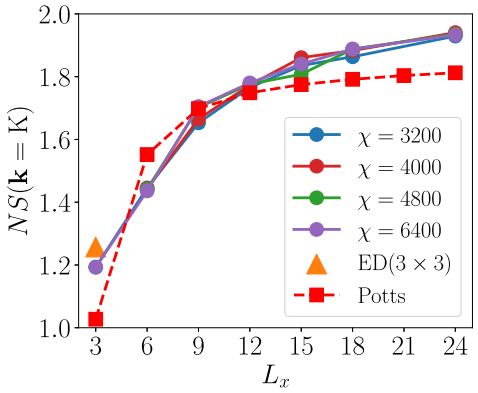

FIG. 5. Rescaled peak intensity at the K point for our unpolarized system on lattices of size $L_x \times 3$, with $6 \leq L_x \leq 24$, obtained using DMRG (circles joined by solid lines). We also show the 3×3 result obtained using ED (yellow triangle). We compare these results with the behavior of the three-state Potts model on lattices of size $L_x \times 3$, with $6 \leq L_x \leq 24$ (squares and dotted lines), which in $d = 2$ is known to sit on a KT transition between algebraic and long-range magnetic correlations.

values of $S(\mathbf{k}=K)$ when the classical correlators are scaled as appropriate for semiclassical behavior [i.e., by $(S^z)^2=1/4$ instead of $S(S+1)=3/4$, see End Matter] and a similar dependence of $S(\mathbf{k}=K)$ on system size. Spin correlations in our model exhibit slow decay and oscillations also consistent with $\sqrt{3}\times\sqrt{3}$ order (see Supplemental Material [31]). Indeed, the slightly larger value, and faster growth, of the correlations with system size in Fig. 5 for our problem compared to the Potts model hints at the possibility of a single hole inducing long-range semiclassical $\sqrt{3}\times\sqrt{3}$ magnetic order. We note however that the identification of ordered states on the kagome lattice is notoriously challenging and we cannot rule out other possibilities, in particular if they involve large unit cells or more complex order parameters.

Conclusions—We presented a study of kinetic frustration in a singly doped Mott insulator on the kagome lattice. Close to full polarization, we uncover a complex interplay between flat-band localization and polaron formation resulting in nonmonotonic band-mass behavior. We developed a description of the polarons in terms of resonant-valence-bond states characteristic of the same system on a Husimi cactus [12]. When these RVB polarons are large enough to encircle hexagonal plaquettes on the lattice, we found that their band mass diverges within our numerical precision, and they appear to relocalize in a disorder-free system. As we moved toward the unpolarized limit, the RVB polaron description becomes less useful and the spin correlations appear to morph toward semiclassical $\sqrt{3}\times\sqrt{3}$ order.

Valence bond physics has been shown to play a key role in kinetic frustration on line-graph lattices [4,5] such as the 2D checkerboard and 3D pyrochlore lattices. In these cases, the unpolarized limit of our problem results in an RVB spin liquid state [6,13]. Interestingly, the fully polarized limit of these lattices hosts once again flat bands and compact localized states. Therefore it will be interesting to extend our Letter of the behavior of RVB polarons and their nonmonotonic band mass in these systems as one varies polarization.

Another important direction for future work is the case when multiple holes are present in the system. This opens the door to polaron-mediated interactions between the holes, and possible binding, pairing, and phase separation effects. Our preliminary study of the 2H10S system indeed suggests an effective attraction between the holes.

One also wonders whether the addition of farther-range hopping terms could lead to itinerant bipolarons, as recently found on the triangular lattice [30].

Acknowledgments—We thank C. D. Batista, C. Glittum, José J. Baldoví, F. Pollmann, and A. Wietek for insightful discussions. We are particularly indebted to C. Glittum for sharing with us preliminary results on an $L_x=3$, $L_y=3$ kagome system. This work was supported in part by the Engineering and Physical Sciences Research Council (EPSRC) Grant No. EP/V062654/1 (C. C.), and the Deutsche Forschungsgemeinschaft via the cluster of excellence ctd.qmat (EXC 2147, Project No. 390858490) and SFB 1143 (Project No. 247310070).

Data availability—The data that support the findings of this study are available from the corresponding author upon reasonable request.

[1] D. J. Thouless, Exchange in solid ^{3}He and the Heisenberg Hamiltonian, Proc. Phys. Soc. London **86**, 893 (1965).
[2] Y. Nagaoka, Ferromagnetism in a narrow, almost half-filled s band, Phys. Rev. **147**, 392 (1966).
[3] H. Tasaki, Extension of Nagaoka's theorem on the large-U Hubbard model, Phys. Rev. B **40**, 9192 (1989).
[4] A. Mielke, Exact results for the $U=\infty$ Hubbard model, J. Phys. A **25**, 6507–6515 (1992).
[5] U. Brandt and A. Giesekus, Hubbard and Anderson models on perovskitelike lattices: Exactly solvable cases, Phys. Rev. Lett. **68**, 2648–2651 (1992).
[6] H. Tasaki, Exact resonating-valence-bond ground state and possibility of superconductivity in repulsive Hubbard models, Phys. Rev. Lett. **70**, 3303–3306 (1993).
[7] K. Penc and R. Lacaze, $spl(2,1)$ dynamical supersymmetry and suppression of ferromagnetism in flat-band double-exchange models, Europhys. Lett. **48**, 561 (1999).
[8] J. O. Haerter and B. S. Shastry, Kinetic antiferromagnetism in the triangular lattice, Phys. Rev. Lett. **95**, 087202 (2005).
[9] S. V. Iordanskiĭ and A. V. Smirnov, Magnetic structures in the Hubbard model with nearly half-filled band for non-alternating lattices, Sov. Phys. JETP **52**, 981 (1980).
[10] C. N. Sposetti, B. Bravo, A. E. Trumper, C. J. Gazza, and L. O. Manuel, Classical antiferromagnetism in kinetically frustrated electronic models, Phys. Rev. Lett. **112**, 187204 (2014).
[11] Z. Zhang and C. Glittum, Resonating valence bond ground states on corner-sharing simplices, arXiv:2507.10471.
[12] K.-S. Kim, Exact hole-induced resonating-valence-bond ground state in certain $U=\infty$ Hubbard models, Phys. Rev. B **107**, L140401 (2023).
[13] C. Glittum, A. Štrkalj, D. Prabhakaran, P. A. Goddard, C. D. Batista, and C. Castelnovo, A resonant valence bond spin liquid in the dilute limit of doped frustrated Mott insulators, Nat. Phys. **21**, 1211 (2025).
[14] H.-C. Jiang, T. Devereaux, and S. A. Kivelson, Holon Wigner crystal in a lightly doped kagome quantum spin liquid, Phys. Rev. Lett. **119**, 067002 (2017).
[15] Z. Zhu, D. Sheng, and A. Vishwanath, Doped Mott insulators in the triangular-lattice Hubbard model, Phys. Rev. B **105**, 205110 (2022).
[16] S. A. Chen, Q. Chen, and Z. Zhu, Proposal for asymmetric photoemission and tunneling spectroscopies in quantum simulators of the triangular-lattice Fermi-Hubbard model, Phys. Rev. B **106**, 085138 (2022).
[17] I. Morera, M. Kanász-Nagy, T. Smolenski, L. Ciorciaro, A. Imamoğlu, and E. Demler, High-temperature kinetic magnetism in triangular lattices, Phys. Rev. Res. **5**, L022048 (2023).
[18] Y. Tang, L. Li, T. Li, Y. Xu, S. Liu, K. Barmak, K. Watanabe, T. Taniguchi, A. H. MacDonald, J. Shan *et al.*,

Simulation of Hubbard model physics in WSe_2/WS_2 moiré superlattices, Nature (London) **579**, 353 (2020).
[19] L. Ciorciaro, T. Smoleński, I. Morera, N. Kiper, S. Hiestand, M. Kroner, Y. Zhang, K. Watanabe, T. Taniguchi, E. Demler *et al.*, Kinetic magnetism in triangular moiré materials, Nature (London) **623**, 509 (2023).
[20] M. Xu, L. H. Kendrick, A. Kale, Y. Gang, G. Ji, R. T. Scalettar, M. Lebrat, and M. Greiner, Frustration-and doping-induced magnetism in a Fermi-Hubbard simulator, Nature (London) **620**, 971 (2023).
[21] M. Lebrat, M. Xu, L. H. Kendrick, A. Kale, Y. Gang, P. Seetharaman, I. Morera, E. Khatami, E. Demler, and M. Greiner, Observation of Nagaoka polarons in a Fermi–Hubbard quantum simulator, Nature (London) **629**, 317 (2024).
[22] M. L. Prichard, B. M. Spar, I. Morera, E. Demler, Z. Z. Yan, and W. S. Bakr, Directly imaging spin polarons in a kinetically frustrated Hubbard system, Nature (London) **629**, 323 (2024).
[23] A. Mielke, Ferromagnetism in the Hubbard model on line graphs and further considerations, J. Phys. A **24**, 3311 (1991).
[24] A. Mielke, Exact ground states for the Hubbard model on the kagome lattice, J. Phys. A **25**, 4335 (1992).
[25] C. Lanczos, An iteration method for the solution of the eigenvalue problem of linear differential and integral operators, J. Res. Natl Bur. Stand. **45**, 255 (1950).
[26] A. Wietek, L. Staszewski, M. Ulaga, P. L. Ebert, H. Karlsson, S. Sarkar, L. Shackleton, A. Sinha, and R. D. Soares, XDiag: Exact diagonalization for quantum many-body systems, SciPost Phys. Codebases 70 (2026).
[27] J. Hauschild *et al.*, Tensor network Python (TeNPy) version 1, SciPost Phys. Codebases 41 (2024).
[28] With subtle exceptions due to band touching at the Γ point [29].
[29] D. L. Bergman, C. Wu, and L. Balents, Band touching from real-space topology in frustrated hopping models, Phys. Rev. B **78**, 125104 (2008).
[30] S.-S. Zhang, W. Zhu, and C. D. Batista, Pairing from strong repulsion in triangular lattice Hubbard model, Phys. Rev. B **97**, 140507 (2018).
[31] See Supplemental Material at http://link.aps.org/supplemental/10.1103/zbxv-vtq8 for additional numerical data and an independent analysis of the 12-site system identified in the main text. It also includes the additional Refs. [32,33].
[32] R. R. P. Singh and D. A. Huse, Ground state of the spin-1/2 kagome-lattice Heisenberg antiferromagnet, Phys. Rev. B **76**, 180407(R) (2007).
[33] R. Baxter, Colorings of a hexagonal lattice, J. Math. Phys. (N.Y.) **11**, 784 (1970).
[34] These states are superpositions of the hole at any of the sites on the cluster, and all electrons paired into nearest-neighbor singlets. A property of the Husimi cactus is that the singlet pattern is uniquely determined by the hole position.
[35] We added a small uniform pinning potential around a given hexagonal plaquette to select one of the GSs (see End Matter).
[36] This result is further supported by ED on a finite region of the lattice given by the sites where the reversed spins are localized. The correlators obtained from the ED GS are indeed in good agreement with the ones obtained from DMRG on the full system (see Supplemental Material [31]).
[37] Linear system sizes multiple of 3 were chosen to ensure commensurability.
[38] D. A. Huse and A. D. Rutenberg, Classical antiferromagnets on the kagomé lattice, Phys. Rev. B **45**, 7536 (1992).
[39] G.-W. Chern and R. Moessner, Dipolar order by disorder in the classical Heisenberg antiferromagnet on the kagome lattice, Phys. Rev. Lett. **110**, 077201 (2013).

End Matter

Methods—We used ED to obtain our main results for 1HnS, $n = 1, \ldots, 5$. We were able to access sizes up to 12×12 (namely, $3L_xL_y = 432$ sites) for $n = 1$, up to 9×9 for $n = 2$, up to 6×6 for $n = 3$, up to 5×5 for $n = 4$, and up to 5×4 for $n = 5$, all with periodic boundary conditions. As the K points in the BZ can only be accessed for linear system sizes that are integer multiples of 3, it was not possible to read off directly the band maxima in our largest systems for $n = 4$, 5. Rather than presenting the 3×3 or 6×3 data, where finite size effects are severe, we chose to present the 5×5 and 5×4 data, respectively, for $n = 4$ and $n = 5$, as a lower bound estimate of the bandwidth (see Supplemental Material [31]).

To obtain the data shown in Fig. 4(d), we added a pinning potential $\epsilon \sum_{i \in p} \hat{n}_i$ with p identifying the six sites around a given hexagonal plaquette, and $\epsilon = 10^{-6}$. This allowed us to select one of the 12-site 1H5S GSs in our ED. We checked that the chosen value of ϵ was sufficiently small not to affect the nature of the selected GS. We further verified this against DMRG results (see Supplemental Material [31]).

For $n \geq 5$, we conducted DMRG calculations in YC geometries with system sizes 8×4 and 8×6 using the TeNPy package [27], apart from $n = 5$ where an additional 12×4 simulation was performed [Fig. 4(c)]. In all DMRG calculations, we used cylindrical geometry with open boundary conditions in the x direction. DMRG calculations were considered converged when the energy difference between two consecutive sweeps fell below 10^{-8}, and the entanglement entropy difference below 10^{-6}, with a maximum sweeping count of 200. The bond dimension was set to $\chi = 6400$. We contrasted results on different system sizes to check that they agree within statistical error, up until the point where the polaron is large enough for boundary effects to become important.

In the unpolarized sector, we used ED for $L_x = L_y = 3$ (with periodic boundary condition), and DMRG for $L_y = 3$ and L_x ranging from 6 to 24 (with open boundary conditions in the x direction); $\sqrt{3} \times \sqrt{3}$ order requires L_x and L_y to be integer multiples of 3 to avoid incommensurability issues. The calculations were considered converged when the energy difference between two consecutive sweeps fell below 10^{-7}, and the entanglement entropy difference below 10^{-5}, with a maximum sweeping count of 200.

Husimi cluster states—In order to gain insight into the structure of the 1HnS polarons, we identify the possible Husimi cactus shapes consisting of n adjacent triangles on the kagome lattice (see Fig. 3 in the main text). We diagonalize the Hamiltonian in Eq. (1) restricted to these clusters, and identify the GSs. In agreement with Ref. [12], the GS on each of these clusters is a unique superposition (with real positive amplitudes) of all possible hole positions across the cluster and the electrons paired into nearest-neighbor singlets. These GSs are then extended to states of the full system ($|\psi_{\mathrm{HC}}\rangle$) by taking their tensor product with polarized spins on all other sites. Crucially, for $n = 1, 2, 3, 4$, the states $|\psi_{\mathrm{HC}}\rangle$ are mutually orthogonal. The projection values (absolute values of the inner products) onto the GS of the original system (obtained numerically using ED) are reported in the main text, after accounting for translation and rotation invariance. For $n = 4$ there are three symmetry-inequivalent Husimi cluster shapes, as illustrated in Fig. 3. In a 5×5 system, we find that the one lowest in energy is the most ramified (treelike) one, and it leads to a 93% projection onto the GS, as reported in the main text. The other two shapes have higher energy and lead to 9% and 0.4% projection (top and bottom shape in the inset of Fig. 3, respectively).

For $n = 5$, there are many different Husimi cluster shapes. The maximally curved linear arrangements discussed in the main text are the only ones where the Husimi cactus states $|\psi^{(i)}_{\mathrm{HC}}\rangle$, $i = 1, \ldots, 6$—corresponding to different clusters obtained by rotations around the central hexagon—are nonorthogonal (the dimer-singlet basis is over-complete on the 12-site cluster). While each such state has energy -3.03, their superposition $|\psi_{12-\mathrm{sites}}\rangle = \sum_{i=1}^{6}(-1)^i|\psi^{(i)}_{\mathrm{HC}}\rangle$ in fact has lower energy: $\langle\psi_{12-\mathrm{sites}}|\mathcal{H}|\psi_{12-\mathrm{sites}}\rangle = -3.10$. This is lower than the energy of the most ramified configuration, $E = -3.08$. We therefore take $|\psi_{12-\mathrm{sites}}\rangle$ as our Husimi cluster variational 1H5S ground state, and find that it has an excellent overlap with the exact result from ED, as reported in the main text. By comparison, the most ramified configuration has only a 0.1% projection (in a 4×4 system). A further discussion of this state can be found in Supplemental Material [31], where an in-depth study of the 12-site cluster is also presented.

Potts model—The data presented in Fig. 5 include our Letter of the three-state Potts model, with Hamiltonian $H_{\mathrm{Potts}} = \sum_{\langle ij\rangle} \delta_{\sigma_i\sigma_j}$, $\sigma_i = 0, 1, 2$. The ground state ensemble is extensively degenerate and consists of all states without identical nearest neighbors. We used Monte Carlo simulations with loop updates to sample the ground states at zero temperature. The algorithm starts with a configuration satisfying the nearest-neighbor constraint and iteratively updates it by identifying closed loops with alternating states and exchanging them. We present results with open boundary conditions in the x direction in Fig. 5. In calculating the spin-spin correlations and the spin structure factor in Eq. (2), we treat each of the Potts states as classical spins of length $1/2$ (as appropriate for semiclassical order). Therefore, identical Potts states give $\mathbf{S} \cdot \mathbf{S} = 1/4$ whereas different states give $\mathbf{S} \cdot \mathbf{S} = -1/8$. This choice guarantees that a ferromagnetic classical and a ferromagnetic quantum spin-$1/2$ system give the same value of $S(\mathbf{0})$.

The Potts model is known to sit at the KT transition separating a $\sqrt{3} \times \sqrt{3}$ ordered phase and an algebraically correlated phase [38,39], and it provides a natural benchmark for an analysis of semiclassical $\sqrt{3} \times \sqrt{3}$ correlations. In the Supplemental Material [31], we further show spin correlation function data suggesting that kinetic frustration on the kagome lattice leads to more pronounced $\sqrt{3} \times \sqrt{3}$ order than the Potts model (at least on our quasi-1D cylindrical geometry).